ISSN 0010-9525, Cosmic Research, 2025, Vol. 63, Suppl. 1, pp. S289–S296. © Pleiades Publishing, Ltd., 2025.
Russian Text © The Author(s), 2024, published in Sovremennyie Problemy Distantsionnogo Zondirovaniya Zemli iz Kosmosa, 2024, Vol. 21, No. 4, pp. 263–274.

Formation of Resonant Scattering on Excited Ions of Oxygen and Nitrogen Atoms in Lidar Studies of the Atmosphere

V. V. Bychkov*

Institute of Cosmophysical Research and Radio Wave Propagation, Far East Branch, Russian Academy of Sciences, Paratunka, 684034 Russia

**e-mail: vasily.v.bychkov@gmail.com*

Received July 8, 2024; revised July 8, 2024; accepted July 8, 2024

Abstract—The results of the analysis of lidar data obtained in Kamchatka (53° N, 158° E) in 2008–2022 are presented. Atmospheric sounding was carried out in the altitude range of 25–600 km at wavelengths of 532 and 561 nm. The appearance of increased scattering in the altitude range of 200–400 km was detected. It is shown that it is caused by resonant scattering on excited ions of nitrogen and oxygen atoms. Under night conditions, such ions are created in the process of ionization of the main gas components of the atmosphere during the precipitation of energetic electrons. It is shown that the process of excitation of ions in the ground state does not play any significant role in the formation of the lidar signal. Resonant scattering at these altitudes appears in the process of ionization of the main gas components—N_2, O_2, and O. A mechanism for the formation of a lidar signal of resonant scattering on excited ions is proposed. A general scheme is proposed for assessing the potential efficiency of laser radiation when choosing a wavelength for lidar research of the atmosphere. The meaning of the scattering coefficient in the thermosphere is discussed.

Keywords: atmosphere, ionosphere, lidar, scattering

DOI: 10.1134/S001095252560221X

INTRODUCTION

The use of resonant scattering in the propagation of laser radiation in the upper atmosphere was first proposed in 1964. The history of the development of the method in the following 10 years is given, for example, in the review [9]. Based on the work of various authors, the resonant scattering cross sections were determined for transitions of the gaseous components of the atmosphere He, NO, N_2^+, and N_2 with radiation in the range of 300–1100 nm and for electron transitions in metallic atoms and ions of Na, K, Li and Ca with radiation in the visible range.

For metallic ions, the resonant scattering cross section is of the order of 10^{-13} m^2 sr^{-1}, which is 13–14 orders of magnitude greater than the molecular scattering cross sections for the main gas components of the atmosphere. For gas components, the resonant scattering cross sections have values from 10^{-12} up to 10^{-21} m^2 sr^{-1} through different transitions. High values of the scattering cross section make it possible to obtain a return lidar signal from the thermosphere altitude region. Most of the works published today use scattering by metallic ions, which is explained by their large cross section and appearance at altitudes of 80–140 km. Lidar systems have been created that allow measuring ion content, temperature, wind speed, and their dynamics in changing geophysical conditions [13–15, 20].

The lidar station in Kamchatka, consisting of a Brilliant-B laser (532.08 nm) and a Newtonian telescope with a mirror diameter of 60 cm, began operating in the fall of 2007. The appearance of aerosol in an area of 25–80 km was studied. The background signal was calculated based on the upper strobes of the main signal in the altitude range greater than 100 km. It was discovered that on some days "anomalous" signal behavior was observed: the total lidar signal retained an inclination to the altitude axis of up to 500–600 km. In the process of studying the background signal and the possible aftereffect of the photomultiplier tube (PMT) in March and September 2008, correlations were discovered between the lidar signal from the 200–300 km region and the critical frequency foF2 of the ionosphere [4]. In the same work, a correlation was found between the position of the lidar signal maximum and the value of the effective height of the F2 layer. In Fig. 1, the following correlations are presented, constructed based on the results of observations on March 28, 2008. Similar correlations were obtained during the autumn equinox on September 5 and 6, 2008 [12].

The dynamics of lidar data for January–February 2008, summarized over layers of ~5 km in the meso-

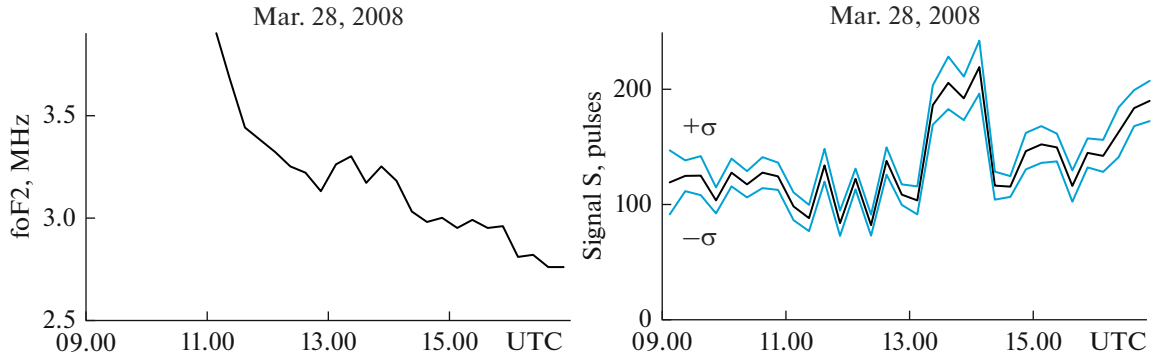

Fig. 1. Critical frequency of the F2 layer of the ionosphere and the lidar signal summed over a region of 200–300 km [4].

pause region, was studied. Strange correlations between lidar signals and ionospheric parameter f_{min} have been discovered [5], which meant a correlation of the lidar signal with the free electron content at these altitudes.

An increase in ionospheric parameters foF2 and f_{min} means an increase in the content of free electrons in the region of the maximum of the F2 layer (foF2) and the mesopause (f_{min}). The results obtained allowed us to suggest that resonant scattering by ions was observed. Lines of excited ions of the nitrogen atom, falling within the laser emission spectrum, were detected. After upgrading the lidar with a dye laser, the 561.106-nm line of the excited oxygen atom ion was selected as the most effective by laser pulse energy.

EQUIPMENT

The 2017 observations used a dual-frequency lidar with an Nd:YAG laser generating radiation at a wavelength of 532.08 nm and a dye laser generating radiation at a wavelength of 561.106 nm at a frequency of 10 Hz. The main parameters of the lidar used in the experiments are given in Table 1. The lidar diagram is given in publication [6] and is not reproduced.

METHODS OF MEASUREMENT AND SIGNAL PROCESSING

To eliminate the illumination of the photomultiplier tube from near-field signals in both receiving channels, electronic blocking of the photomultiplier tube with a pulse duration of 140 μs was used. This corresponds to the exclusion of data in the first ~25 km. The received signals are stored as binary files with 10-s accumulation, which allows for further summation over any time interval. Usually they are 15 min in accordance with the operating mode of the ionosonde.

The background signal was measured starting from 20 ms after sending each laser pulse for 4 ms with a step of 10 μs. In 2017, sounding was carried out at wavelengths of 532.08 and 561.106 nm. With these settings, three emission lines were included in the laser emission spectrum. These lines correspond to dipole transitions [16]:

$$\begin{aligned}
&\text{for the oxygen atom ion:} && 2s^2 2p^2\left(^1\mathrm{S}\right)3s + h\nu\,(561106\ \text{nm}) - 2s^2 2p^2\left(^3\mathrm{P}\right)4p && \mathrm{O}^{*+}\\
&\text{for the nitrogen atom ion:} && 2s2p^2\left(^4\mathrm{P}\right)3p + h\nu\,(532095\ \text{nm}) - 2s2p^2\left(^4\mathrm{P}\right)3d && \mathrm{N}^{*+}\\
& && 2s2p\left(^3\mathrm{P}^\circ\right)3p + h\nu\,(532087\ \text{nm}) - 2s2p\left(^3\mathrm{P}^\circ\right)3d && \mathrm{N}^{*++}.
\end{aligned} \qquad (1)$$

Table 1. Lidar equipment

Transmitter 1	Transmitter 2	Receiver
Nd:YAG Brilliant-B Laser	TDL-90 Dye Laser	60-cm telescope mirror
Pulse energy 400 mJ	YG-982E pump laser	PMT H8259-01
Wavelength 532.08 nm	Pulse energy 100 mJ	M8784-01 counters
Spectrum width 0.040 nm	Wavelength 561.106 nm	Height step 1.5 km
Pulse duration 5 ns	Spectrum width 0.025 nm	Passband of light filters 1 nm
Beam divergence 0.5 mrad	Pulse duration 10 ns	

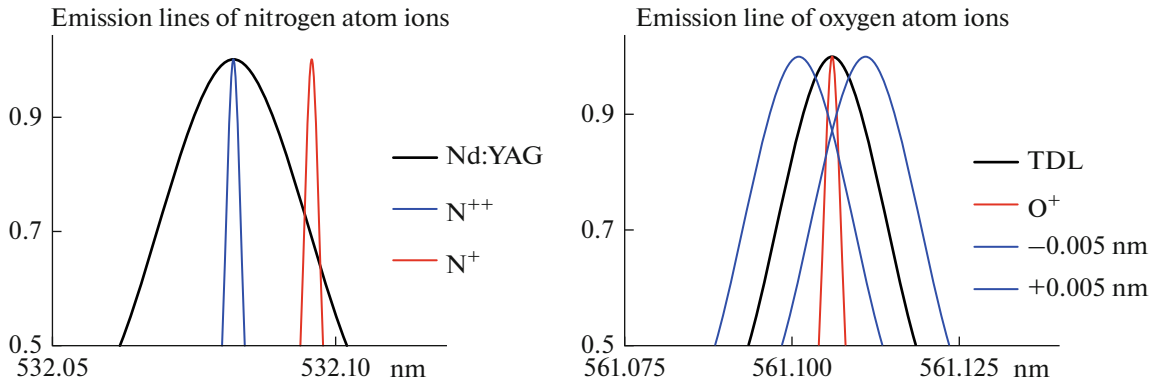

Fig. 2. Emission lines of excited nitrogen and oxygen ions in the emission spectra of Nd:YAG and TDL lasers.

The remaining transition parameters can be easily found by following the link in the spectroscopy reference book. During the reverse transition, resonant scattering can be recorded.

The state of the ionosphere was recorded based on the results of measurements by the Parus-A ionosonde. The computers that control the operation of the ionosonde and lidar are synchronized in time via GPS. The primary lidar data processing program removes signals received during ionosonde operation to eliminate possible interference with the lidar receiving system.

In Fig. 2, the location of excited ion lines (1) in laser spectra is shown [3, 11]. The lines shown in Fig. 2 are selected taking into account the bandwidth of the laser radiation and the Doppler broadening of the line. At an altitude of 300 km, the temperature is ~800 K and the lines for N^+ and O^+ ions are broadened and equal ~0.004 nm. Dotted lines on the right side in Fig. 2 show a shift in the laser emission spectrum relative to the oxygen ion emission line due to a possible error in the TDL laser calibration. It is assumed that the laser wavelength is set with an accuracy of 0.01 nm. The line of doubly ionized nitrogen ions falls in the center of the laser emission band, but the content of such ions is small. The main contribution to the lidar signal is made by N^{*+} and O^{*+} ions.

EXPERIMENTAL DATA

The introduction presents the results of recording resonant scattering (see Fig. 1) at a wavelength of 532 nm in the thermosphere. The values of the total signal in the region of 200–300 km for 15 min of accumulation were of the order of ~10^2. During the period from August to November 2017, seven cases of thermospheric backscatter were recorded on both lidar channels. A characteristic feature of the data obtained during this period is scattering in the region of 200–400 km and its absence at altitudes of 100–200 km. Moreover, the values of the total lidar signal in the 200–400 km region were more than an order of magnitude higher than the values observed in 2008.

In Fig. 3, the spatiotemporal distribution of the return signal received on August 28, 2017, is shown. The background signal has been subtracted. The profile is smoothed in height using the moving average method with a 4.5-km window. The signal values are multiplied by the coefficient kH^2, where H is altitude (in km) and $k = 10^{-4}$. Total lidar signal S, accumulated overnight, and the same signal S_n, normalized by coefficient kH^2, are presented at the bottom of Fig. 3. Normalization to the square of the height corresponds to the actual decrease of the real signal with increasing height. With the selected coefficient value $k = 10^{-4}$, at an altitude of 100 km, the signal coincides with the actually recorded signal, thereby improving the visual perception of the data.

These and other events [11] observed in August–November 2017 are similar in their visual representation in the thermosphere. In all cases, except for August 3 (the first recorded appearance of the layer in 2017), the geomagnetic situation was calm. According to the Paratunka geomagnetic observatory, local 3-h K-indices were equal to (2 1 1 **0 1** 2 2 1), (2 3 2 **2 2** 1 2 1), and (1 1 1 **0 2** 1 2 1) on August 28, September 5, and 23, respectively. The numbers in bold indicate the values recorded during lidar measurements.

The background signal was stable, amounting to 20–30 counts in the nitrogen line over 15 min of accumulation. In the oxygen line it is approximately three times higher, 60–90 counts. In all cases, the total signal values at a wavelength of 532 nm were 20–30% higher than at a wavelength of 561 nm. The appearance of light-scattering layers in all cases was accompanied by the precipitation of electrons into the atmosphere. This was confirmed by the appearance of F-scattering on ionograms, an increase in foF2 values under night conditions, and data from direct measurements of electron fluxes on the MetOp-1 and MetOp-2 meteorological satellites, which flew east and then west of Kamchatka during lidar observations.

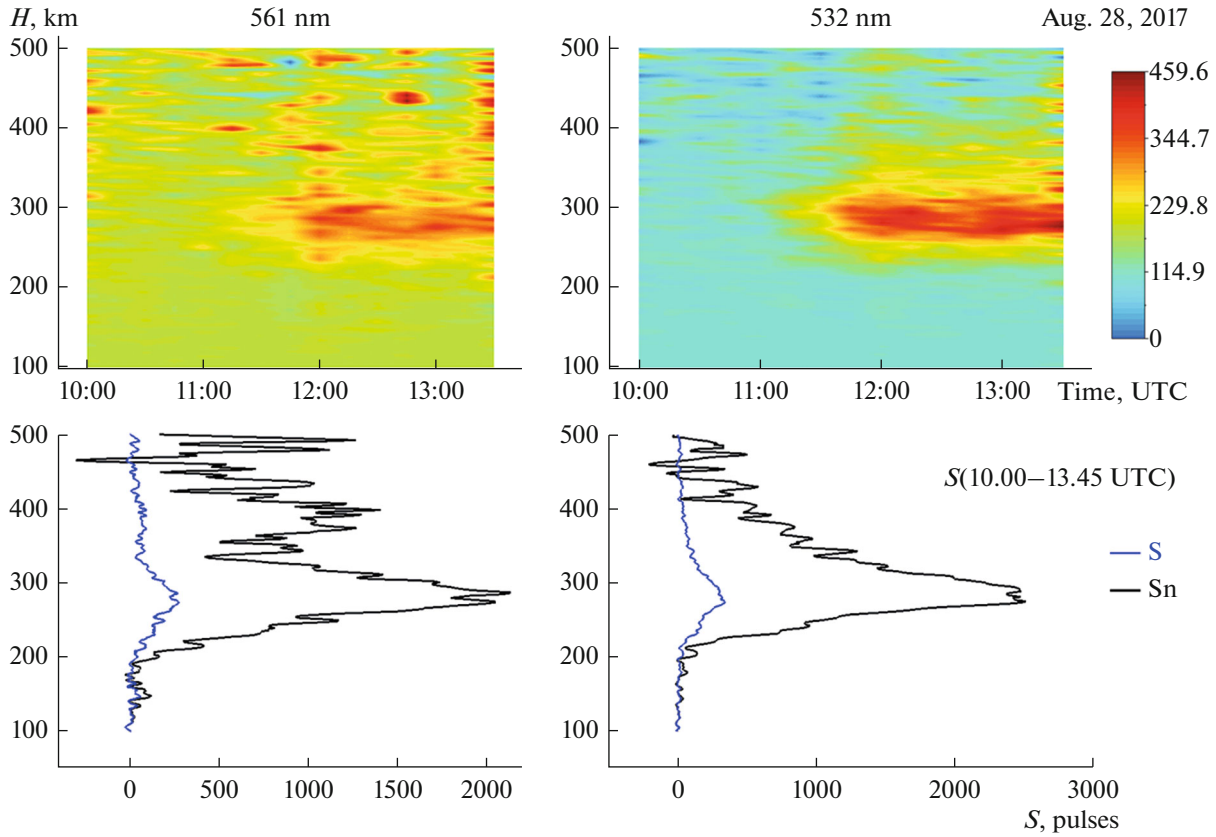

Fig. 3. Lidar signal—background in the region of 100–500 km (*above*), total signal S and normalized signal S_n (*below*), obtained on August 28, 2017.

CHARACTERISTIC FEATURES OF LIDAR DATA

The following main features can be noted in all lidar sounding data obtained in August–November 2017.

1. The magnitude of the lidar signal at 561 nm was expected to be several times greater than the signal at 532 nm, since the O^+ ion content at altitudes of 150–400 km is approximately two orders of magnitude higher than that of N^+ ions [19]. Lidar observations showed that the total signal over night at 532 nm was typically 20–30% greater than at 561 nm.

2. The height of the scattering signal maxima does not coincide with the position of the F2 layer maximum. The lidar signal is maximum at altitudes of 280–290 km in all cases. According to ionosonde data, for example, on September 5, 2017, the maximum of the F2 layer during registration of the light-scattering layer was at altitudes of 300–350 km.

3. The main maximum of the signal is well approximated by the ionization rate profile of a monoenergetic beam of precipitating electrons with an energy of 330 eV [3, 17].

4. Increased scattering of light, forming a second local maximum at altitudes of 350–450 km (see Fig. 3) noted for all signals at a wavelength of 561 nm. In all cases, at a wavelength of 532 nm, with increasing height, the signal monotonically decreased from its maximum value.

Let us recall the basic properties of the ionosphere, which will be needed later. The main processes that determine the formation of the ionosphere are the ionization reactions of the N_2, O_2, and O components by photon or electron impact with the formation of N_2^+, O_2^+, and O^+ ions. Study [19] presents the results of ionospheric modeling in the altitude range of 100–400 km. The model parameters were adjusted for measurement data from the *AE-C* (*Atmosphere Explorer-C*) satellite. The paper presents diagrams of photochemical processes and the rates of formation of components of the lower thermosphere. The most important results of this work for us can be formulated as follows:

• the determining process that forms the appearance of an N^+ ion in the ground state is the ionization of molecular nitrogen;

• the main process that forms $O^+(^4S)$ ions in the ground state is the ionization of molecular and atomic oxygen;

• the rate of formation of O^+ ions is approximately 1.5 times higher than that of N^+ ions;

• more than half of all N^+ and O^+ ions are born in an excited state.

MECHANISM OF FORMATION OF A RESONANT SCATTERING SIGNAL

The formation of a resonant scattering signal consists of the absorption of a photon by an ion, the transition of the ion to an upper level, followed by a reverse transition and emission at the same frequency. The lower level states in transitions (1) are also excited. Lifetime of an excited ion τ is defined as

$$\tau = 1/\left(\sum A_{jk} + \nu\right), \quad (2)$$

where A_{ik} are the Einstein coefficients for spontaneous transitions and ν is the frequency of collisions of ions with neutrals. Summation of Einstein coefficients A_{ik} is produced for all states into which radiative transitions are possible [10]. For the region above 100 km, we can set $\nu = 0$, since the frequency ν of ion collisions at these altitudes is $<5 \times 10^3\ s^{-1}$, which is much less than the frequencies of radiative transitions. Searching for all such states in database [16], we obtain values of τ equal to 1.06, 1.42, and 12.82 ns for O^+, N^{++}, and N^+, respectively. These values are close to the values of laser pulse durations T_{pulse} at wavelengths of 532 and 561 nm, which are equal to 5 and 10 ns, respectively.

In an arbitrary thin layer of the atmosphere, the content of excited ions is proportional to the rate of formation of these ions, multiplied by lifetime τ of this state. In addition, the interaction will involve ions that were born in this layer during time the laser pulse strobe was in it T_{pulse}. The signal should be proportional to the ion production rate multiplied by the sum of the pulse duration and the excited ion lifetime.

As a first approximation, it is possible to evaluate signal N as follows:

$$N \sim V\left(\tau + T_{pulse}\right)P, \quad (3)$$

where P is the probability of interaction of an ion with a photon of a laser pulse and V is the rate of formation of ions in the desired state. The probability of interaction of the resulting ion can be determined by the value $\sigma N\tau$, where $N\tau$ is the number of "useful" photons that have passed through a unit area during ion lifetime τ, multiplied by scattering cross section σ. We will call "useful photons" those with a wavelength in the region of Doppler line broadening (see Fig. 2). If $\sigma N\tau$ is greater than 1, then the probability of absorption of a photon is close to 1; otherwise, it is equal to $\sigma N\tau$.

The resonant scattering cross section in the classical representation convenient for calculations [8] is equal to $\sigma = 3/(2\pi)\,\lambda^2$, where λ is the wavelength. Substituting the values of 532 and 561 nm, we obtain 1.35×10^{-13} and $1.5 \times 10^{-13}\ m^2$, respectively. The use of collimators reduces beam divergence by seven to eight times, to 0.08 mrad. The illuminated surface area at an altitude of 300 km will be equal to 350 m^2.

The photon energies are 2.33 and 2.3 eV or 3.72×10^{-19} and 3.68×10^{-19} J for wavelengths of 532 and 561 nm. Number of "useful" photons $N\tau$ in the pulse, taking into account the data of Table 1 and Fig. 2, equals 40 and 15 mJ, or $\sim 1.0 \times 10^{17}$ and 0.4×10^{17} photons for nitrogen and oxygen ions, respectively. Taking into account the losses in the lidar transmission path (5–10% on the four surfaces of the two collimator lenses and the output mirror) and scattering in the atmosphere (20%), number of photons $N\tau$ passing through 1 m^2 over the lifetime of the ion, will be 1.28×10^{14} and 5.1×10^{-13} for 532 and 561 nm. To estimate the probability of interaction between a photon and an ion, we obtain the values of $\sigma N\tau$ equal to 17.2 and 0.75 for pulses of 532 and 561 nm. A more detailed, although not complete, calculation is given in the work [3, 11].

When using a lidar with the parameters presented in the table, at an altitude of 300 km, the probability of absorption of a photon by an excited ion of atomic nitrogen is close to unity with a multiple (17 times) energy reserve of the laser pulse. For oxygen ions, the absorption probability is 0.75. This means that all excited ions in the strobe will participate in the process of photon absorption at pulse energies greater than 100 mJ for nitrogen ions and greater than ~150 mJ for oxygen ions. As the pulse energy increases, the signal will not increase. It will depend only on the ionization rate.

If we assume that the rates of formation of excited O^+ and N^+ ions in the state of the lower level of transitions (1) are equal, then the ratio of the number of absorbed photons N_{561}/N_{532}, calculated using formula (3), will be equal to 0.42. This means that each pair of laser pulses will raise 2.5 times more nitrogen ions than oxygen ions to the upper level. The experimentally obtained signal ratio is equal to $N_{561}/N_{532} \sim 0.8$. This does not mean that the rate of oxygen ion formation should be approximately twice as high.

The lidar signal is determined by the proportion of ions that have returned to the initial state of the lower level of transitions (1) with radiation at the resonant wavelength. To estimate this fraction, it is necessary to find all states into which radiative transitions from the upper level are possible, and, based on the values of the Einstein coefficients, estimate the probability of transitions. In the wavelength range of 50–1500 nm, eight nitrogen lines and ten oxygen lines were found, corresponding to possible transitions from upper levels in relation (1). It can be assumed that the fraction of ions leaving the upper level for each allowed transition will be proportional to the contribution of the Einstein coefficient of this transition to the total sum that determines the lifetime of the state in accordance with formula (2). The energy level diagram of these transitions is shown in Fig. 4.

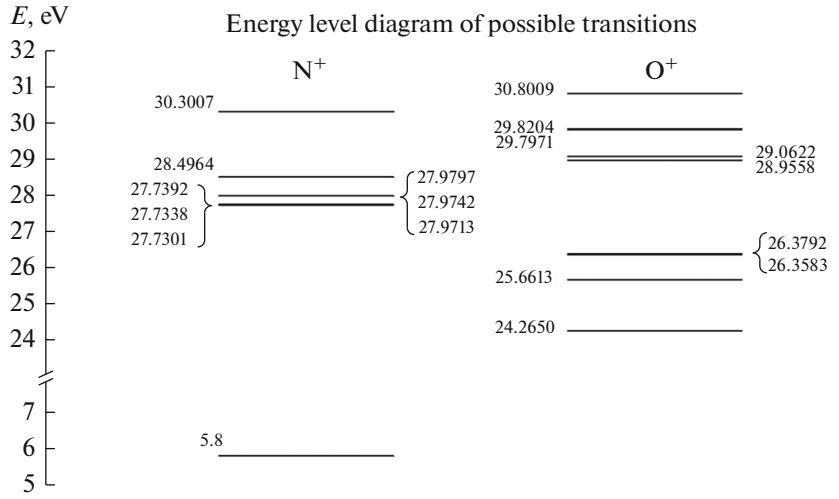

Fig. 4. Diagram of radiative transitions of excited ions of oxygen and nitrogen atoms from upper-level states to (1).

Calculations showed that about 2.5% of oxygen ions and ~0.6% of nitrogen ions will participate in the transition with radiation at resonant frequencies. For a ratio of 2.5 : 1 for the number of nitrogen ions raised to the upper level to oxygen, the proportion of nitrogen ions returning with resonance radiation must be reduced by approximately four times. For resonant transitions we obtain the relation $N_{532}/N_{561} = 0.625$. Taking into account the lidar data for the rates of appearance of the lower level states of transitions (1), we obtain $V_N/V_O = 1/0.625/0.8 = 2$. The rate of formation of lower level states of transitions (1) for nitrogen ions should be twice as high as for oxygen ions. This ratio of the rates of appearance of excited states is realistic and can explain the observed ratio of signals at wavelengths of 532.08 and 561.106 nm.

Ions in the lower level states of transitions (1) can be formed by excitation of existing ions or by creation in the process of ionization of neutral components of the atmosphere. At an altitude of 300 km, the N_2, O_2, N, and O content is equal to 1.5×10^8, 4×10^6, 1.5×10^7, and 6×10^8 cm^{-3}, respectively [18], the night content of N^+ and O^+ equals 10^2 and 10^4 cm^{-3}. Cross sections of ion excitation and atom ionization of the same order [1, 2]. Only the process of ionization of atomic components will make an order of magnitude greater contribution to the rate of formation of N^{*+} and O^{*+} than the process of excitation of existing ions. The main contribution to the formation of the F2 layer of the ionosphere is made by the ionization process of N_2, O_2, and O. Atomic N^+ and O^+ are formed as a result of photochemical transformations of N_2^+ and O_2^+, including their dissociation.

The second maximum on the scattering profile on oxygen ions (see Fig. 3) is present in all recorded cases of layer appearance. It appears as a result of the ionization of atomic oxygen. At an altitude of 400 km the content of O and O_2 about 10^8 and 10^5 cm^{-3}. They make up 90 and 0.1% of the total content of atmospheric components. Contents of O^+ are from four to five orders of magnitude smaller. Excitation of existing ions does not play a significant role in the formation of the lidar signal at all altitudes of the F2 region of the ionosphere.

ON THE ROLE OF ION PRE-EXCITATION PROCESSES

In general, the equations for the population of an excited level are p have the form

$$dN_p/dt = G_p - L_p, \quad (4)$$

where N_p is the population level of p and G_p and L_p are the rates of arrival and departure of ions from adjacent levels.

Level transition speeds i to the level p have the form $k_{ip} N_e N_i + A_{jk} N_i$, where k_{ip} is the rate constant of additional excitation by electron impact from level i on p, N_e is electron concentration, and N_i is concentration of ions at the level i.

To determine the influence of these transitions, it is necessary to solve a system of equations of form (4). It is also necessary to consider ionization and recombination reactions and add equations for electron temperature and density. For our purposes, there is no need to solve this problem. It is sufficient to evaluate the influence of these processes on the lidar signal. The lidar signal depends on both the content (population) and the arrival rate of excited ions. Let us consider the evolution of additional ionization, "raised" to the upper level by a pair of laser pulses.

The lifetime of the upper-level states of transitions (1) is determined by formula (2) and is 0.22 and 15 ns for nitrogen and oxygen ions. During this time, all ions "raised" by the lidar pulses will move to lower levels

(see Fig. 4), including the original ones, in the amount of 0.6 and 2.5% of nitrogen and oxygen ions. For ions that have returned to their original state, repeated transitions to the upper level according to scheme (1) are possible if the pulse gate is still at the location of the ion. However, even if all the returning ions are raised back to the upper level, only 0.6 and 2.5% of the population of newly raised ions will return to the original lower level. Moreover, 98.2% of nitrogen ions will pass into the ground state with radiation at a wavelength of 50.6 nm. This process decays each time by two orders of magnitude, and its contribution to the lidar signal can be neglected.

Under night conditions, the contribution of additional excitation of ions at lower levels (see Fig. 4) radiation at wavelengths resonant for the upper level can be ignored.

Let us also evaluate the possibility of additional excitation due to collisions with free electrons of the ionosphere. The frequency of elastic collisions of electrons with ions can be estimated using the formula $\nu_{ei} = 20\left(N_i/T_e^{3/2}\right)$, where N_i is ion concentration and T_e is temperature (http://www.astrolyceum.lpi.ru/Seminar/Collision.pdf). For $N_i = 10^4$ cm^{-3} and $T_e = 800$ K, we obtain the value $\nu_{ei} = 10$ Hz. For ions in states with a principal quantum number of 3–4, the lifetime values lie in the range of 1 ns–1 μs. The obtained estimate of the collision frequency of 10 Hz means that the ion content is from five to six orders of magnitude insufficient to ensure the process of additional excitation.

As for the additional excitation by precipitating electrons. In the previous section it was shown that both the population and the rate of ion arrival at the excited lower levels of transitions (1) are provided mainly by the ionization process of N_2, O_2, and O. The contribution of the excitation process of existing ions is several orders of magnitude smaller. This also applies to excited states at lower levels (see Fig. 4). The contribution to the signal from the process of additional excitation by precipitating electrons can be ignored.

Thus, we can draw a general conclusion that, at altitudes of 100–500 km, the influence of postexcitation processes on nitrogen and oxygen ions can be neglected. The proportion of ions returning to their original state with radiation at resonant frequencies of 532 and 561 nm will not change noticeably. In general, for other transitions and conditions, such an assessment must be carried out.

ON THE SCATTERING COEFFICIENT

The attenuation coefficient for the propagation of laser radiation is understood as the coefficient $\alpha(\upsilon, H)$, in the Bouguer–Lambert–Beer law in differential form for a plane wave, having the form [7]: $dI(\upsilon) = -I(\upsilon)\alpha(\upsilon, H)dH$, Where $I(\upsilon)$—intensity of radiation with frequency υ, W/cm^2; $\alpha(\upsilon, H) = \beta a + \beta m + \beta p$—attenuation coefficient; βp — absorption coefficient; βa, βm—coefficients of aerosol and molecular scattering.

As already noted, at a wavelength of 532 nm, for pulse energies greater than 100 mJ and a duration of 5 ns, at altitudes of 300 km, the probability of interaction of ions with pulse photons is close to unity. The same resonant scattering signal will be obtained and, accordingly, the same attenuation d$I(\upsilon)$ for different radiation intensities $I(\upsilon)$.

The difference between aerosol and resonance scattering is that the aerosol target can participate in several scattering events of photons from a single laser pulse. In resonant scattering, the target is destroyed upon the first interaction with a photon. At an altitude of more than 100 km, where $\beta a = \beta m = 0$, resonant scattering can be observed. According to the Beer–Lambert–Bouguer law, the scattering coefficients for it will be different for different laser radiation energies; from a certain value of $I(\upsilon)$, the return signal does not depend on the laser pulse energy.

In fact, the process of forming a resonant scattering signal on excited oxygen and nitrogen ions is a process of absorption of radiation and scattering at the same wavelength of only a small fraction of the adsorbed radiation. Above 100 km, $\beta m = 0$ and the calculation of the scattering coefficient using any approximations of the average atmosphere does not make sense.

CONCLUSIONS

An analysis of lidar data and the geophysical environment accompanying the appearance of light-scattering layers in the thermosphere was conducted. A conclusion is made about resonant scattering, and a mechanism for the formation of a resonant scattering lidar signal is proposed. The following conclusions can be drawn.

• Resonance scattering at wavelengths of 532.095 and 561.106 nm occurs on excited ions of atomic nitrogen and oxygen, generated in the process of ionization of oxygen, nitrogen, and atomic oxygen molecules.

• The process of ionization of atomic oxygen can manifest itself in resonant scattering at altitudes greater than 300 km. Below, it is masked by the contribution of molecular components.

• The influence on the signal of the excitation process of O^+ and N^+ ions in the ground state is negligible. Lidar data do not contain significant information about their content in the atmosphere; lidar does not "see" ions in the ground state. Resonance scattering provides information about the appearance of ionization sources in the atmosphere.

• The proposed mechanism for generating a lidar signal can be used to evaluate the potential efficiency

of a lidar when selecting an operating wavelength for lidar studies of the atmosphere.

ACKNOWLEDGMENTS

I would like to express my gratitude for consultations on spectrometry issues to A.A. Ilyin, candidate of physical and mathematical sciences, senior researcher at the Institute of Automation and Control Processes of the Institute of Automation and Control Processes of the Far East Branch of the Russian Academy of Sciences. The work was carried out using the equipment of the Center for Collective Use (CCU) of the Institute of Cosmophysical Research and Radio Wave Propagation (IKIR) of the Far East Branch of the Russian Academy of Sciences (IKIR FEB RAS, CCU "North-East Heliogeophysical Center" 558279, Unique Scientific Installation 351757).

FUNDING

The work was carried out within the framework of a state assignment of the IKIR FEB RAS, topic registration no. 124012300245-2.

CONFLICT OF INTEREST

The author of this work declares that he has no conflicts of interest.

REFERENCES

1. Avakyan, S.V., Voronin, N.A., and Serova, A.E., The role of Rydberg atoms and molecules in the upper atmosphere, *Geomagn. Aeron. (Engl. Transl.),* 1997, vol. 37, no. 3, pp. 331–335.
2. Andreev, G.V., Calculation of the ionization cross-section for electron impact of hydrogen and nitrogen atoms, *Fiz.-Khim. Kinet. Gaz. Din.,* 2010, vol. 9, pp. 263–264. http://chemphys.edu.ru/issues/2010-9/articles/161/.
3. Bychkov, V.V. and Seredkin, I.N., Resonance scattering in the thermosphere as an indicator of superthermal electron precipitation, *Atmos. Ocean. Opt.,* 2021, vol. 34, no. 1, pp. 26–33. https://doi.org/10.1134/S1024856021010048
4. Bychkov, V.V. and Shevtsov, B.M., Dynamics of lidar reflections of the Kamchatka upper atmosphere and its connection with phenomena in the ionosphere, *Geomagn. Aeron. (Engl. Transl.),* 2012, vol. 52, pp. 797–804. https://doi.org/10.1134/S0016793212060047
5. Bychkov, V.V., Perezhogin, A.S., Perezhogin, A.S., et al., Observations of aerosol occurrence in the middle atmosphere of Kamchatka in 2007–2011, *Atmos. Ocean. Opt.,* 2012, vol. 25, no. 3, pp. 228–235. https://doi.org/10.1134/S1024856012030037
6. Bychkov, V.V., Seredkin, I.N., and Marichev, V.N., Scattering on excited ions as a reason for detecting imaginary aerosols in the middle atmosphere, *Atmos. Ocean. Opt.,* 2021, vol. 34, no. 2, pp. 104–111. https://doi.org/10.1134/S1024856021020032
7. Zuev, V.V., *Lidarnyi kontrol' stratosfery* (Lidar Control of the Stratosphere), Novosibirsk: Nauka, 2004.
8. Konstantinov, O.V. and Matveentsev, A.V., Giant resonant scattering cross sections of electromagnetic wave by an electron in a metal or semiconductor cluster, *Tech. Phys. Lett.,* 2010, vol. 36, no. 11, pp. 1032–1033. https://doi.org/10.1134/S1063785010110179
9. Kostko, O.K., Use of laser radar in atmospheric investigations (review), *Sov. J. Quantum Electron.,* 1975, vol. 5, no. 10, pp. 1161–1189. https://doi.org/10.1070/QE1975v005n10ABEH011998
10. Shefov, N.N., Semenov, A.I., and Khomich, V.Yu., *Izluchenie verkhnei atmosfery—indikator ee struktury i dinamiki* (Radiation of the Upper Atmosphere—An Indicator of Its Structure and Dynamics, Moscow: GEOS, 2006.
11. Bychkov, V.V., Resonant scattering by excited gaseous components as an indicator of ionization processes in the atmosphere, *Atmosphere,* 2023, vol. 14, no. 2, pp. 271–287. https://doi.org/10.3390/atmos14020271
12. Bychkov, V.V., Nepomnyashchiy, Y.A., Perezhogin, A.S., and Shevtsov, B.M., Lidar returns from the upper atmosphere of Kamchatka on observations in 2008–2014, *Earth Planets Space,* 2014, vol. 66, p. 150. https://doi.org/10.1186/s40623-014-0150-6
13. Collins, R., Hallinan, T., Smith, R., and Hernandez, G., Lidar observations of a large high-altitude sporadic Na layer during active aurora, *Geophys. Res. Lett.,* 1996, vol. 23, no. 24, pp. 3655–3658. https://doi.org/10.1029/96GL03337
14. Collins, R., Li, J., and Martus, C., First lidar observation of the mesospheric nickel layer, *Geophys. Res. Lett.,* 2015, vol. 42, no. 2, pp. 665–671. https://doi.org/10.1002/2014GL062716
15. Kawahara, T., Nozawa, S., Saito, N., et al., Sodium temperature/wind lidar based on laser-diode-pumped Nd: YAG lasers deployed at Tromsø, Norway (69.6° N, 19.2° E), *Opt. Express,* 2017, vol. 25, no. 12, pp. A491–A501. https://doi.org/10.1364/OE.25.00A491
16. Kramida, A., Ralchenko, Yu., Reader, J., et al., NIST atomic spectra database (ver. 5.5.2), Gaithersburg, MD: Natl. Inst. Stand. Technol., 2018. https://physics.nist.gov/asd.
17. Rees, M.H., Auroral ionization and excitation by incident energetic electrons, *Planet. Space Sci.,* 1963, vol. 11, no. 10, pp. 1209–1218. https://doi.org/10.1016/0032-0633(63)90252-6
18. Picone, M., Hedin, A.E., and Drob, D., NRLMSISE-00 Model, 2001. https://ccmc.gsfc.nasa.gov/modelweb/atmos/nrlmsise00.html.
19. Richards, P.J., Reexamination of ionospheric photochemistry, *J. Geophys. Res.,* 2011, vol. 116, no. A8, p. A08307. https://doi.org/10.1029/2011JA016613
20. Tsuda, T., Nozawa, S., Kawahara, T., et al., Decrease in sodium density observed during auroral particle precipitation over Tromsø, Norway, *Geophys. Res. Lett.,* 2013, vol. 40, no. 17, pp. 4486–4490. https://doi.org/10.1002/grl.50897